Structural investigation of a chaperonin in action reveals how nucleotide binding regulates the functional cycle

Guillaume Mas, Jia-Ying Guan, Elodie Crublet, Elisa Colas Debled, Christine Moriscot, Pierre Gans, Guy Schoehn, Pavel Macek, Paul Schanda, Jérôme Boisbouvier

STRUCTURAL BIOLOGY

Structural investigation of a chaperonin in action reveals how nucleotide binding regulates the functional cycle

Guillaume Mas*, Jia-Ying Guan, Elodie Crublet†, Elisa Colas Debled, Christine Moriscot, Pierre Gans, Guy Schoehn, Pavel Macek†‡, Paul Schanda‡, Jerome Boisbouvier‡

Chaperonins are ubiquitous protein assemblies present in bacteria, eukaryota, and archaea, facilitating the folding of proteins, preventing protein aggregation, and thus participating in maintaining protein homeostasis in the cell. During their functional cycle, they bind unfolded client proteins inside their double ring structure and promote protein folding by closing the ring chamber in an adenosine 5′-triphosphate (ATP)–dependent manner. Although the static structures of fully open and closed forms of chaperonins were solved by x-ray crystallography or electron microscopy, elucidating the mechanisms of such ATP-driven molecular events requires studying the proteins at the structural level under working conditions. We introduce an approach that combines site-specific nuclear magnetic resonance observation of very large proteins, enabled by advanced isotope labeling methods, with an in situ ATP regeneration system. Using this method, we provide functional insight into the 1-MDa large hsp60 chaperonin while processing client proteins and reveal how nucleotide binding, hydrolysis, and release control switching between closed and open states. While the open conformation stabilizes the unfolded state of client proteins, the internalization of the client protein inside the chaperonin cavity speeds up its functional cycle. This approach opens new perspectives to study structures and mechanisms of various ATP-driven biological machineries in the heat of action.

INTRODUCTION

Chaperones, proteins that assist folding and stabilization of other proteins, are essential for cellular homeostasis and viability. Chaperonins, a particular class of chaperones also noted hsp60 in the following, form a giant barrel-like structure composed of two back-to-back stacked rings. While group I chaperonins, such as bacterial GroEL, require a co-chaperonin lid (GroES) to cap the ring chamber, group II chaperonins, present in the eukaryotic cytosol and in archaea, are composed of subunits with a built-in helical protrusion which closes the folding chamber. Biochemical studies have provided limited structural information on key steps of the chaperonin functional cycle and mechanism of protein folding (*1*–*4*). Hsp60 chaperonin undergoes large-scale adenosine 5′-triphosphate (ATP)–dependent conformational changes to promote folding of the client protein within a large chamber. Structures of open and closed states (*5*–*9*) have provided static snapshots of steps along the cycle, but the conformational dynamics of the active ATP-fueled chaperone, as well as the interactions with client proteins being refolded, have remained elusive. Nuclear magnetic resonance (NMR) spectroscopy is the method of choice to study proteins in solution and is, in principle, able to observe conformational changes, interactions, and dynamics under functional conditions. However, the site-specific observation of proteins as large as chaperonin, 1 MDa, remains a significant challenge due to the extensive line broadening of NMR signals in large proteins. Furthermore, retaining the protein in a functional state throughout a structural investigation is complicated by the rapid consumption of ATP, thereby leading to inactivation and inhibition of the ATP-dependent machinery.

To overcome these methodological limitations, we have developed an ATP regeneration system directly inside an NMR tube to keep the ATP concentration constant and to prevent the accumulation of adenosine 5′-diphosphate (ADP), thereby maintaining the chaperonin in a steady working condition powered by ATP hydrolysis. We furthermore elaborated a combined methyl-specific labeling approach to probe the different conformational states of the chaperonin and its client proteins. This combination of methods allows us to probe, on the structural level, the different states involved in the functional cycle of active hsp60 processing client proteins while the chaperonin is being powered by ATP hydrolysis (*10*, *11*). We provide quantitative measures of the thermodynamics and kinetics of the transitions between the open and closed conformations and reveal how the chaperonin affects the folding/unfolding equilibrium of the client protein. Specifically, we find that hsp60 acts as a holdase of unfolded proteins until activation by ATP. ATP binding closes the chaperonin cavity, while the ATP hydrolysis rate controls the timing of the closed state, during which encapsulated proteins can refold for a period of ~17 s. After ATP hydrolysis, the chamber reopens during the ADP residence time (~10 s), which allows release of folded protein and client proteins to be reloaded before the start of a new cycle. Our results reveal how nucleotides and client protein binding regulate the transition between different conformations populated during the hsp60 functional cycle. We anticipate this work to be a starting point to obtain insights into the mechanisms of various chaperones. Furthermore, our approach opens new perspectives for the study of structures and mechanisms of ATP-powered biomolecular machines.

University of Grenoble Alpes, CNRS, CEA, IBS, F-38000 Grenoble, France.
*Present address: Biozentrum University of Basel, Klingelbergstrasse 70, 4056 Basel, Switzerland.
†Present address: NMR-Bio, F-38000 Grenoble, France.
‡Corresponding author. Email: macek@nmr-bio.com (P.M.); paul.schanda@ibs.fr (P.S.); jerome.boisbouvier@ibs.fr (J.B.)

RESULTS

ATP binding closes the chaperonin cavity

We have chosen to study the conformations, nucleotide binding, and client protein interaction of a group II chaperonin from the

hyperthermophilic *Pyrococcus horikoshii* (*12*). This hsp60 chaperonin is a homohexadecameric assembly (Fig. 1, A and B), that is, a simplified mechanistic model of its eukaryotic heterohexadecameric counterpart. Furthermore, with an optimal functional temperature above 60°C, where NMR relaxation properties are more favorable, site-specific NMR information can be obtained at the level of individual residues under physiologically relevant conditions. However, studying a 1-MDa protein assembly is challenged by the low sensitivity and resolution associated with rapid NMR spin relaxation (*13*, *14*). By combining selective valine and methionine methyl labeling (*15*, *16*) with methyl–transverse relaxation optimized spectroscopy (TROSY) experiments (*17*, *18*), we have obtained high-quality NMR spectra, allowing us to probe the structure and dynamics at 62 individual sites evenly dispersed throughout the structure of the chaperonin (Fig. 1, B and C, and figs. S1 and S2). In nucleotide-free or ADP-bound states, chaperonins are in an open state allowing the access of client proteins to the cavity (Fig. 1A) (*19*–*22*). However, the event that triggers the open-to-closed transition (Fig. 1B) remains a matter of discussion (*4*, *19*, *23*–*26*). Having highly resolved NMR spectra, we probed the conformational states of chaperonin in the presence of different nucleotide ligands. Chemical shift perturbations induced by the binding of ADP and a nonhydrolyzable ATP analog (App-NHp) revealed that M159, located in the vicinity of the nucleotide binding site, exhibits distinct peak positions in the apo and nucleotide-bound states and, thus, directly reports on the occupancy of the binding site (Fig. 1C). Upon binding of App-NHp, however, the signals of M275 and M279 located in the lid are significantly shifted (fig. S3C), revealing a global conformational change to the closed state (*4*). In contrast, binding of ADP does not affect the signals of these two methionines, confirming that the ADP-bound state, just like the apo state, is in an open conformation (fig. S3B). Negative staining electron microscopy (EM) analysis of the NMR sample (fig. S4) confirmed that App-NHp binding induces the closed conformation. Together, these results show that ATP binding triggers the transition from the open to the closed conformation of the ring, while ADP binding does not affect the closed conformation.

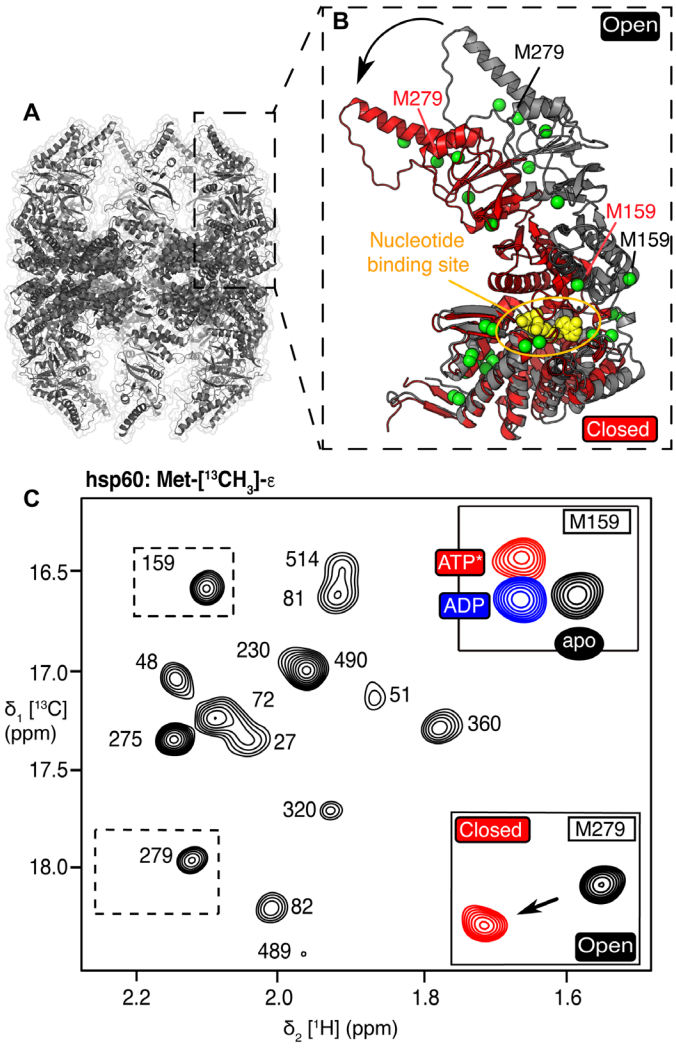

Fig. 1. Methionine-directed methyl NMR allows the identification of the nucleotide binding state and the different chaperonin conformational states. (**A**) Model of the chaperonin structure in the open conformation obtained by homology modeling from Protein Data Bank (PDB 3IZH). (**B**) Magnified view of one hsp60 monomer in open (gray) and closed (red) conformations (obtained by homology modeling from PDB 1Q3R). The methyl groups of methionine residues are represented by green spheres, and the nucleotide in the binding site is represented in yellow. (**C**) 2D ^{1}H-^{13}C methyl-TROSY spectrum of a 12.5 μM U-[^{2}H, ^{15}N], Met-[^{13}CH$_3$] chaperonin sample with the assignment of the methionine residues obtained by combination of a mutagenesis-based approach (fig. S1) with detection of NOEs between methyl groups (fig. S2). The inserts focus on cross peaks of M159 and M279 in the apo state (black) and in the presence of 2 mM ATP analog App-NHp (red, closed state) or ADP (blue, open state).

The open state of chaperonin acts as a holdase of unfolded proteins

Hen egg white lysozyme (HEWL; 14.5 kDa) and malate synthase G (MSG; 82 kDa) were selected as model proteins to observe the interaction of hsp60 with two client proteins with a significant size difference. At 65°C, a temperature close to the optimal conditions for hsp60 activity, HEWL features two sets of NMR resonances corresponding to the unfolded and folded states, which interconvert on a time scale of 350 ms (fig. S5). The addition of chaperonin shifts only the peaks of the unfolded form of HEWL, showing that hsp60 interacts exclusively with the unfolded form (Fig. 2A and fig. S5). Quantitative analysis of the titration data reveals a dissociation constant of 1.6 ± 0.4 μM, with a binding stoichiometry of one unfolded HEWL per chaperonin cavity. NMR-based thermal unfolding studies of HEWL revealed that the presence of hsp60 decreases the melting temperature by 5°C (Fig. 2B and fig. S5), confirming the stabilization of the unfolded state by the chaperonin. The exclusive interaction of hsp60 with the unfolded state is furthermore confirmed by the observation that the translational diffusion coefficients of the unfolded states of HEWL and MSG are shifted to the one of the chaperonin, whereas the folded state of these proteins retain the hydrodynamic properties expected for the globular freely tumbling proteins (Fig. 2C and fig. S6). To determine how these unfolded proteins interact with hsp60, we monitored changes in hsp60 NMR spectra upon the addition of paramagnetically labeled HEWL or MSG (Fig. 2D and fig. S7). Paramagnetic-induced line broadening effects reveal that both unfolded proteins bind to the bottom of the folding chamber nearby the previously proposed sensor loop (Fig. 2E) (*5*). These results demonstrate that hsp60 interacts specifically with unfolded proteins and that the general interaction site for client proteins is located at the base of the chaperonin cavity.

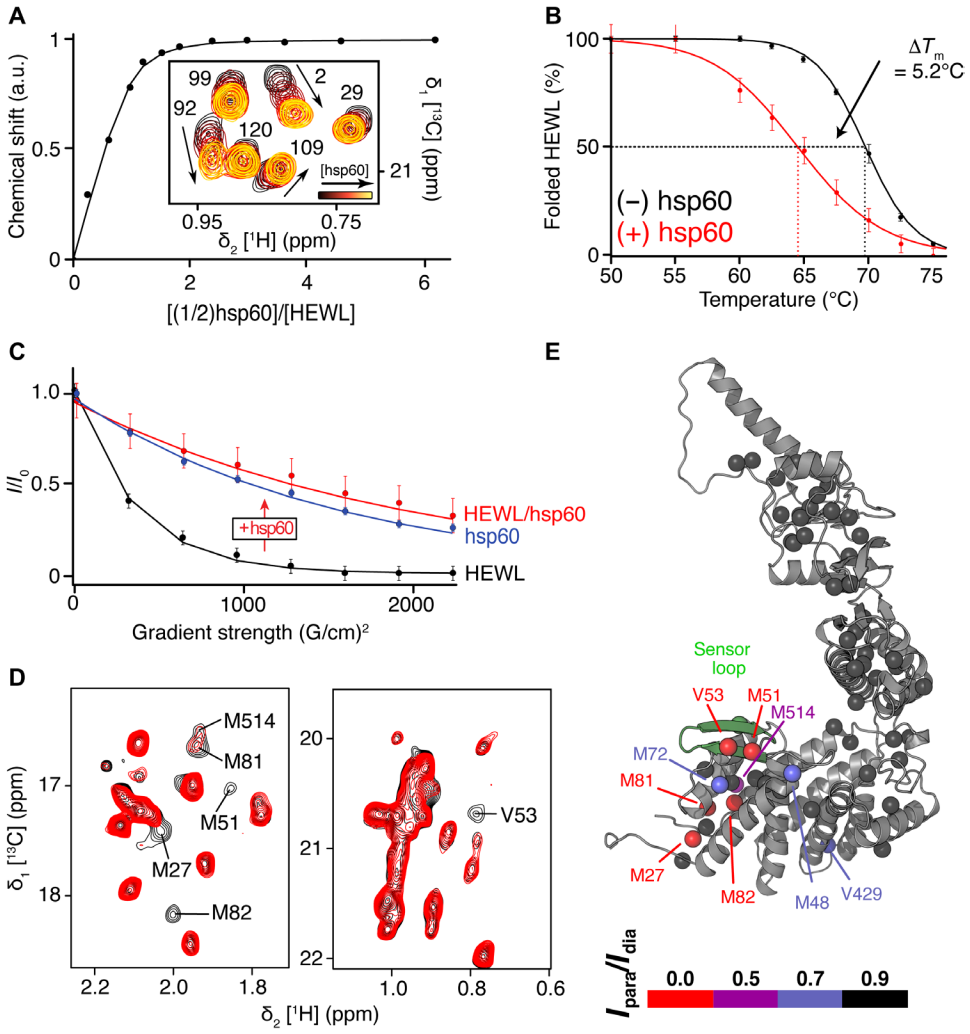

Fig. 2. NMR characterization of the interaction between client protein and hsp60. (**A**) Sum of chemical shift changes of five HEWL methyl signals (V2, I88, V92, V109, and I124) showing a significant shift and no overlap. The inset shows the NMR signal of valine residues of HEWL recorded at 75°C at a constant concentration (31 μM), and an increasing concentration of perdeuterated hsp60 assembly (0 to 97 μM). a.u., arbitrary units. (**B**) Evolution of the folded population of the HEWL between 50° and 75°C without (black) and with (red) hsp60 (two equivalents of HEWL per chaperonin). The melting temperatures (T_m) are indicated by vertical dotted lines. (**C**) Translational diffusion properties of hsp60 alone (blue), unfolded HEWL alone (black), and in the presence of hsp60 (red) characterized by diffusion-ordered NMR spectroscopy. Derived diffusion coefficients at 65°C (hsp60: $5.8 \pm 0.3 \times 10^{-7}$ cm/s^2; unfolded HEWL with hsp60: $4.4 \pm 1.2 \times 10^{-7}$ cm/s^2; unfolded HEWL alone: $30 \pm 4 \times 10^{-7}$ cm/s^2) reveal that only unfolded HEWL is interacting with hsp60. (**D**) Overlay of the 2D ^{1}H-^{13}C NMR spectra of U-[^{2}H, ^{15}N], Val-[^{13}CH$_3$]^{proS}, Met-[^{13}CH$_3$] methyl–labeled sample of hsp60 with two equivalents of diamagnetic (black) or paramagnetic labeled HEWL (red). (**E**) Model of the monomer of hsp60 in the open conformation showing the residues affected by the paramagnetically labeled client proteins. hsp60 sensor loop is colored in green.

Client protein accelerates the functional cycle of hsp60

To study the system in action under steady-state conditions, without accumulation of the competitive inhibitor ADP (*27*), we implemented an enzymatic system directly inside the NMR sample to ensure continuous rapid regeneration of ATP from ADP and phosphoenol pyruvate (PEP; Fig. 3A). This system keeps the ATP concentration constant, prevents ADP accumulation, and keeps the chaperonin catalytically active at a constant rate (Fig. 3, B and C). Moreover, interleaved NMR data collection of this complex reaction mixture allows to simultaneously monitor the state of the chaperonin and client protein, as well as the concentrations of ATP, ADP, and PEP. The distinct sets of methionine NMR resonances report on the open/closed conformational state (M275 and M279) and type of nucleotide bound (M159; Figs. 1 and 3D), while the Ile, Leu, and Val resonances of HEWL report on the equilibrium of folded and unfolded states of the client protein (Fig. 4A and fig. S8). The population of folded HEWL of ca. 50% in the presence of chaperonin alone increased to 75% when powered by ATP and the ATP regeneration system, demonstrating that the active hsp60 is able to enhance the client protein refolding (Fig. 4B). Furthermore, the comparison of ATPase activity of hsp60 with and without HEWL, quantified from the decay of PEP signals, reveals that the presence of client protein enhances the ATPase activity of hsp60 by 40% from 24.7 ± 0.5 to 36.0 ± 1.5 ATP/min per hsp60 (Figs. 3 and 4C and fig. S9). These observations indicate a mutual activation of protein refolding and cycling of the chaperonin between different functional states.

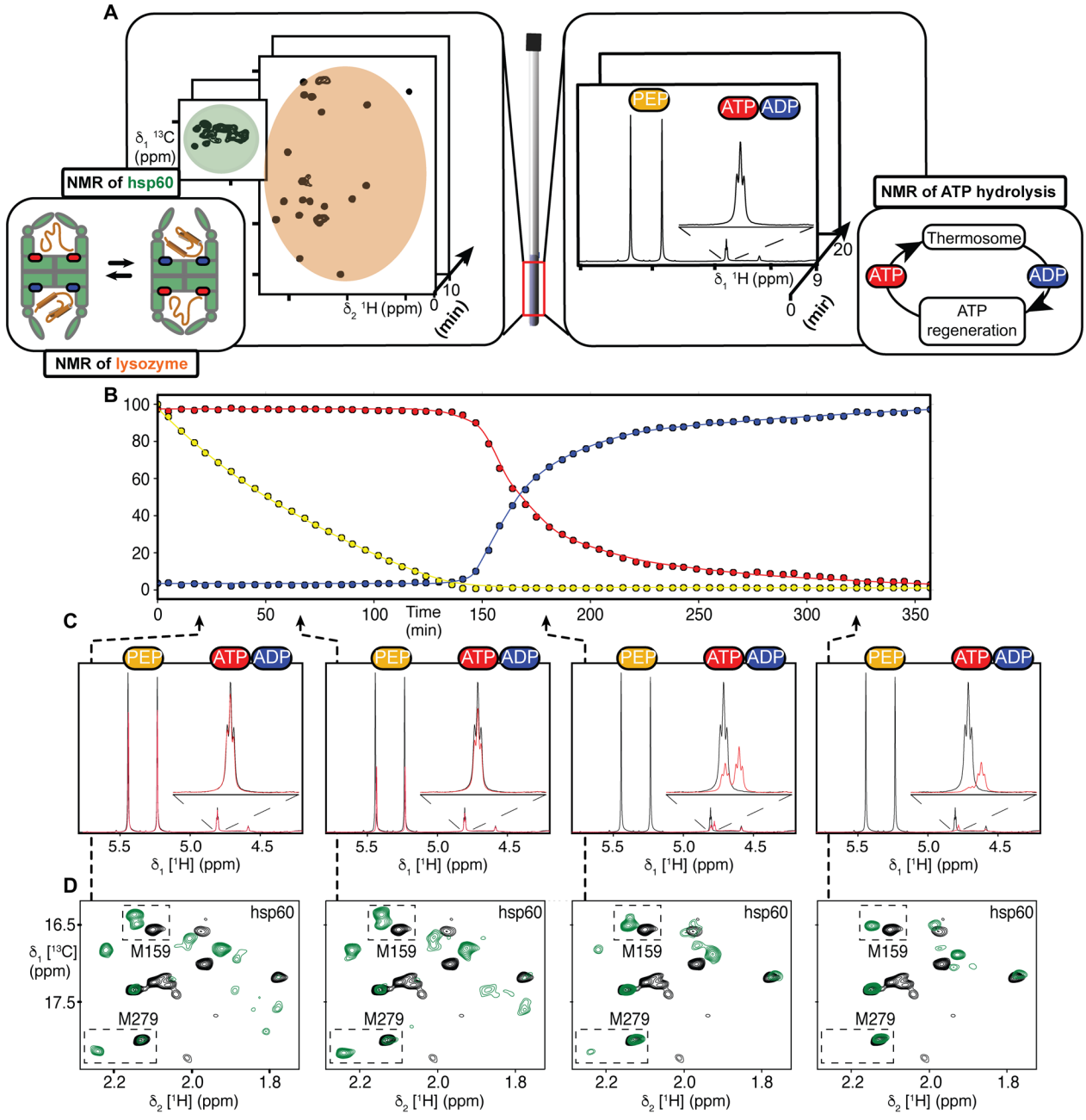

Fig. 3. Real-time NMR study of hsp60 functional cycle in the presence of a client protein. (**A**) Schematic representation of hsp60 functional turnover observed by real-time NMR in the presence of the ATP regeneration system. (**B**) Plot of the PEP, ATP, and ADP concentrations in function of time. Percentage of each species was extracted from the 1D ^{1}H NMR experiment. For PEP, the sum of the initial area of the two signals corresponding to PEP was considered as 100%. For the ATP and ADP, the percentage corresponds to a ratio of the area corresponding to the signal of each molecule. (**C**) 1D ^{1}H NMR spectra recorded at different time points of the experiment [black, reference spectrum at the beginning of the experiment; red, spectrum at the time indicated by an arrow on the graphic (B)]. The zoom on the upper right of each panel corresponds to the signal of ATP and ADP. (**D**) The 2D ^{13}C-^{1}H SOFAST-methyl-TROSY spectra recorded at different times of the experiment corresponding to the hsp60 methionine methyl signals [black, reference spectrum before addition of ATP; green, spectrum at the time indicated by an arrow on the graphic (B)].

Nucleotide binding and hydrolysis control the population of chaperonin conformations

While the chaperonin is being powered by the ATP regeneration system, the NMR reporter of the nucleotide binding state, M159, shows that both the ATP- and ADP-bound states are present in steady state, despite the fact that the concentration of free ADP in solution is negligible (Fig. 4D and fig. S10, A and B). The level of unoccupied binding site is below our detection limit (<3%), showing that the lifetime of nucleotide-free state is negligible compared to the ADP- and ATP-bound states. The reporters of the cavity conformational state (M275 and M279) reveal that there is also a mixture of open and closed states present under these steady-state

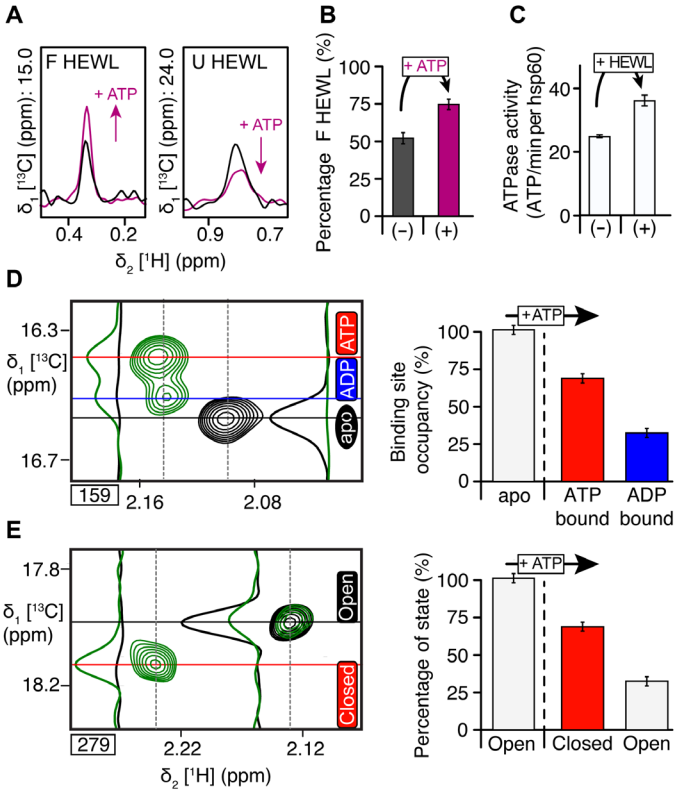

Fig. 4. NMR study of the active hsp60 machinery processing client protein. (**A**) The 1D traces of 2D ^{1}H-^{13}C NMR spectra (fig. S8A), displaying signals of folded (F, left) and unfolded (U, right) states of methyl (Ile-δ1, Val/Leu-proS)–labeled HEWL, recorded before/after the addition of 10 mM ATP. (**B**) Percentage of folded HEWL in the presence of the hsp60 before and after the addition of 10 mM ATP. (**C**) ATPase activity of hsp60 with and without HEWL, calculated from the decrease of the PEP signals (Fig.3 and fig. S9). (**D**) Quantification of the apo, ADP/ATP-bound populations of hsp60 in the presence of HEWL, quantified using intensities of NMR signals of M159 reporter (in black, reference spectrum of apo hsp60; green, spectra after the addition of 10 mM ATP). (**E**) Quantification of the relative populations of open and closed states of chaperonin over time in the presence of HEWL, as derived from the relative intensities of the signals of the two methionines 275 and 279 in the open/closed conformations. Spectra on the left show excerpts of NMR spectra before the addition of ATP (black) and after the addition of ATP (green).

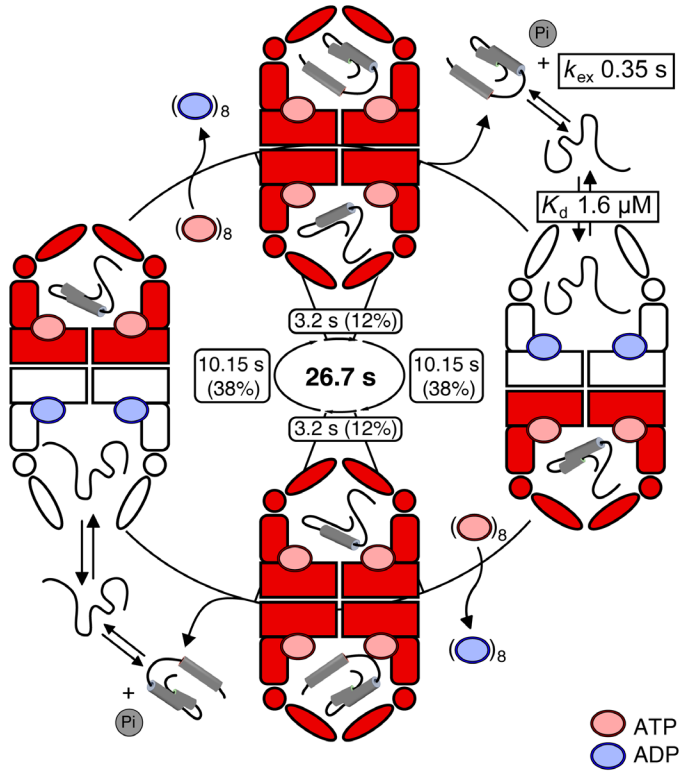

Fig. 5. Model of the functional cycle of chaperonin. Unfolded client protein is stabilized through its interaction with the equatorial domain of the ADP-loaded open hsp60 ring (Fig. 2E and fig. S7). The nucleotide binding sites, initially occupied with ADP, bind ATP without a detectable level of nucleotide-free state. The ATP binding, rather than its hydrolysis, closes the ring, which remains closed until ATP hydrolysis and P_i release. After hydrolysis, the ring reopens but ADP remains bound to the nucleotide binding sites, preventing immediate rebinding of new ATP and chaperonin closing. The chaperonin rings are represented by two symmetric monomers colored in white (inactive ring: ADP bound and open) or red (active ring: ATP bound and closed). The duration for each step of the functional cycle is calculated from the overall ATP hydrolysis rate and the relative populations of open/closed state, as reported in Figs.3 and 4 and fig. S10 and represented on the inside of the circle. K_d, dissociation constant.

conditions (Fig. 4E and fig. S10, C and D). These independent NMR observables allow the determination of population levels of the ATP-bound (62 ± 3%) and ADP-bound states (38 ± 3%), which quantitatively match the ones of the closed and open conformation, respectively (62 ± 3%, 38 ± 3%; Fig. 4, D and E). These relative population levels of open (ADP-bound) and closed (ATP-bound) states of chaperonin are retained also when client protein is present (fig. S10).

DISCUSSION

The chaperonin conformational cycle is driven by ATP; however, its exact role remains a matter of debate (*10*, *11*). A proposed model, in which ATP binding alone is sufficient to close the ring (*4*, *19*, *23*, *24*), was challenged by studies concluding that it is the ATP hydrolysis that drives the ring closing (*3*, *25*, *26*). The quantitative equality of the relative populations of ATP-bound (ADP-bound) states and closed (open) conformations of the chaperonin observed in this study (Fig. 5) implies that ATP binding and chamber closing are intimately linked, and along with the fact that nonhydrolyzable ATP analogs close the hsp60 cavity, these results confirm the view that nucleotide binding, rather than hydrolysis, induces the closure of the ring (Fig. 1B).

This study has also enabled resolution of the cooperativity and conformations of both rings during the adenosine triphosphatase (ATPase) cycle of group II chaperonins. The fact that we observe only two sets of NMR signatures, corresponding to closed/ATP-bound and open/ADP-bound states, leads us to propose that each ring comprising eight subunits acts as a cooperative unit, as proposed earlier (Figs. 3 and 4, D and E, and figs. S9 and S10) (*27*, *28*). This view is corroborated by the absence of mixed conformations within a ring in EM images (fig. S4). Several studies advocated the presence of inter-ring cooperativity in the group II chaperonins, suggesting an alternating mechanism in which one ring is open and the opposite

ring closed (*1*–*3*, *29*, *30*). However, there is also evidence of a nonconcerted mechanism, in particular for the eukaryotic chaperonin CCT (chaperonin containing TCP-1) (*31*, *32*). The extreme model with strict anticooperativity (*3*)—that is, opening of one ring leading to closing of the adjacent ring—predicts the exclusive presence of half-open/half-closed chaperonin particles, that is, populations consisting of 50% open and 50% closed half-rings at each time point. An alternative model based on partial anticooperativity includes doubly closed particles in addition to the half-open/half-closed state (*33*, *34*). The population levels obtained directly from our NMR data of the ATP-powered chaperonin in action allow resolution of these conflicting models. The skewed population levels (62:38 ± 3%) necessarily imply the presence of chaperonin particles that have two closed chambers. Taking into account that nucleotide-free states are absent (Fig. 4D), we propose a modified model (*2*), depicted in Fig. 5, which involves four states along the functional cycle, two of them fully closed and two half-open/half-closed states. The kinetics of ATP processing (Figs. 3 and 4) and the relative populations of states (Fig. 5), detected in our NMR sample, allow determining the average lifetimes of the populated states. With an ATP hydrolysis activity per chaperonin of 36 ATPs/min (Fig. 4C), and assuming that a full cycle consumes 16 ATPs, one catalytic turnover takes 26.7 s. Together with the experimentally observed population levels (Fig. 4, D and E), we can derive that the half-open/half-closed state has a threefold longer lifetime (10.2 s) than the doubly closed state (3.2 s; Fig. 5). The long residence time of the half-open/half-closed state allows the release of the folded proteins and the rebinding of a new unfolded client protein to the chaperonin. In addition, the fact that the ratio of populations in the open and closed conformations equals the ratio of ADP- and ATP-bound states shows that the events following the ATP hydrolysis are subsequently leading to the opening of the chaperonin folding chamber, while the ADP residence time controls the duration of the open state of hsp60 cavity.

Together, our results reveal that nucleotide binding, hydrolysis, and release control the conformational transitions between closed and open states and their relative lifetimes. While the open chaperonin conformation stabilizes the unfolded state of client proteins, its binding inside the cavity speeds up the functional cycle of the chaperonin. The implementation of a fully active chaperoning system, being constantly powered by fresh ATP inside the NMR tube, allows studying biomolecular function in action. This work establishes the feasibility to probe these events at the structural level even in systems as large as 1 MDa. We anticipate our approaches to be applicable to a wide range of protein assemblies, including HSPs (heat shock proteins) involved in cancer (*35*) or in the disaggregation of amyloidogenic proteins (*30*), as well as other large cellular machines in action such as biological motors or polymerases.

MATERIALS AND METHODS

Production and purification of methyl specifically labeled proteins in *Escherichia coli*

Production and purification of specifically methyl-labeled hsp60

E. coli BL21-CodonPlus-(DE3)-RIL cells transformed with a pET-41c plasmid encoding the hsp60 from *P. horikoshii* (also known as thermosome) were progressively adapted in three stages over 24 hours to M9/D_2O medium containing D-glucose-d_7 (2 g/liter; Isotec). As part of our standard labeling protocols, the culture media also contained $^{15}ND_4Cl$ (1 g/liter), but incorporation of ^{15}N in produced samples was not used in this study and these extra ^{15}N spins did not interfere with $^{13}CH_3$-edited NMR experiments reported here. In the final culture, bacteria were grown at 37°C in M9 medium prepared with 99.85% D_2O (Eurisotop). When the optical density (OD) at 600 nm reached 0.6 to 0.7, a solution containing the labeled precursors was added. The precursor solution added for 1 liter of culture medium contained the following: either 100 mg of [αβγ-$^2H_5$, ε-^{13}C]-L-methionine (Cambridge Isotope Laboratories; CIL) for the production of the U-[^2H, ^{15}N], Met-[$^{13}CH_3$] hsp60 sample; or 240 mg of 2-hydroxy-2-[^{13}C]methyl-3-oxo-4,4,4-tri-[^2H]-butanoate (pro-S acetolactate-^{13}C, NMR-Bio), 30 mg of L-leucine-d_{10}, and 100 mg of [α,β,γ-2H5, ε13C]-L-methionine (CIL) for the production of the U-[^2H, ^{15}N], Met-[$^{13}CH_3$], Val-[$^{13}CH_3$]^{proS} hsp60 sample (*15*).

One hour after the addition of the precursors, hsp60 expression was induced by the addition of isopropyl β-D-1-thiogalactopyranoside (IPTG) to a final concentration of 0.5 mM. The induced culture grew for 4 hours at 37°C before harvesting. Cells were lysed by sonication in buffer containing 25 mM Hepes (pH 7.5), 150 mM NaCl, 5 mM $MgCl_2$, and DNase (deoxyribonuclease) (0.01 mg/ml). After the first heat shock step at 80°C, hsp60 was purified using an anion exchange chromatography step (Resource Q, 6 ml, GE Healthcare) followed by a size exclusion chromatography step (HiLoad 16/60 Superdex 200 pg, GE Healthcare). The final yield reached 20 mg/liter of methyl-specific protonated hsp60. The protein was concentrated to final NMR concentration in D_2O buffer [20 mM MES (pH 6.5 uncorrected), 100 mM NaCl, 150 mM KCl, and 25 mM $MgCl_2$]. After concentration of the sample, the ATPase activity of hsp60 was tested using a malachite green assay (Sigma-Aldrich), and the oligomerization state of the particle was controlled using an analytical size exclusion column (CE Agilent Bio SEC-5A 500 Å) and negative staining EM.

Production and purification of hsp60 methionine and valine mutants

Constructs containing valine-to-alanine or methionine-to-leucine single point mutations were generated by an automated molecular biology platform (RoBioMol, Institut de Biologie Structurale) using an automated polymerase chain reaction–based protocol adapted from the QuikChange site-directed mutagenesis method (*36*, *37*). The library of mutants was expressed in parallel in 25 ml of M9/D_2O and labeled on methionine and valine methyl groups following the protocol described above. Purification of hsp60 mutants was done following the protocol described above. The hsp60 mutants were concentrated in D_2O buffer [20 mM MES (pH 6.5 uncorrected), 100 mM NaCl, 150 mM KCl, and 25 mM $MgCl_2$] using centrifugal filter devices (Vivaspin 15, 100,000 MWCO, Vivascience) to a final concentration between 6.25 and 12.5 μM hsp60 (100 to 200 μM monomer).

Production of U-[^2H, ^{15}N], Leu/Val-[$^{13}CH_3$]^{proS}, Ile-[$^{13}CH_3$]^{δ1} HEWL

E. coli BL21-CodonPlus-(DE3) cells transformed with a pET-11a plasmid encoding the HEWL (Addgene plasmid #39233) (*38*) were progressively adapted in three stages over 24 hours to M9/D_2O medium containing $^{15}ND_4Cl$ (1 g/liter) and D-glucose-d_7 (2 g/liter; Isotec). In the final culture, bacteria were grown at 37°C in M9 medium prepared with 99.85 % D_2O (Eurisotop). When the OD at 600 nm reached 0.6 to 0.7, 2-hydroxy-2-[^{13}C]methyl-3-oxo-4,4,4-tri-[^2H]butanoate (proS acetolactate-^{13}C, NMR-Bio) was added at a final concentration of 240 mg/liter 1 hour before induction. Forty minutes later (that is, 20 min before induction), 3,3-[$^2H_2$],4-[^{13}C]-2-ketobutyrate

(NMR-Bio) was added to a final concentration of 60 mg/liter (*15*). One hour after the addition of the first precursors, HEWL expression was induced by the addition of IPTG to a final concentration of 2 mM. The induced culture grew for 3 hours at 37°C before harvesting.

HEWL was purified from inclusion bodies (*38*) and refolded using size exclusion chromatography (*39*). The final yield reached 5 mg/liter of methyl-specific protonated refolded HEWL. The protein was concentrated using centrifugal filter devices (Vivaspin 15, 5000 MWCO, Vivascience) in D_2O buffer [20 mM MES (pH 6.5 uncorrected), 100 mM NaCl, 150 mM KCl, and 25 mM $MgCl_2$].

Production of U-[^{2}H, ^{15}N], Leu/Val-[$^{13}CH_3$]^{proS}, Ile-[$^{13}CH_3$]$^{\delta1}$ MSG

E. coli BL21(DE3) cells were transformed by heat shock with the kanamycin-restricted T7lac promoter–controlled expression plasmid pET21b bearing the MSG gene. Cells were progressively adapted to M9/D_2O media containing $^{15}ND_4Cl$ (1 g/liter) and D-glucose-d_7 (2 g/liter; Isotec) in three stages over 24 hours. In the final culture, the bacteria were grown at 37°C in M9 media prepared with 99.85% D_2O (Eurisotop). When the OD at 600 nm reached 0.7, 2-hydroxy-2-[^{13}C]methyl-3-oxo-4,4,4-tri-[^{2}H]butanoate (pro-S acetolactate-^{13}C, NMR-Bio) was added at a final concentration of 240 mg/liter 1 hour prior to IPTG induction and 40 min later (that is, 20 min prior to induction), and 3,3-[$^2H_2$],4-[^{13}C]-2-ketobutyrate (NMR-Bio) was added to a final concentration of 60 mg/liter (*15*). The induction was performed overnight at 20°C. MSG was purified initially by Chelating Sepharose chromatography (GE Healthcare), followed by gel filtration chromatography (Superdex 200 pg, GE Healthcare). The typical final yield after purification was 80 mg/liter of methyl-specific protonated MSG.

Electron microscopy

Sample (0.1 mg/ml) was applied to the clean side of a carbon layer (between a carbon and a mica layer). The carbon was then floated on stain [2% (w/v) ammonium molybdate (pH 7.4)] and covered by a copper grid. Both were fished and air-dried before loading in the electron microscope. Images were taken with a CM12 microscope (FEI) operating at 120 kV and a nominal magnification of 45,000 times under low-dose conditions on an Orius CCD camera (Gatan).

NMR spectroscopy

All NMR experiments were recorded at specified conditions using 700-, 850-, or 950-MHz Bruker Avance III HD spectrometer equipped with a 1.7-mm (850 MHz) or 5-mm cryogenically cooled pulsed-field gradient triple-resonance probes (700, 850, or 950 MHz).

Two-dimensional (2D) SOFAST-methyl-TROSY NMR experiments (*18*) were recorded with an adjusted duration depending on the final concentration of the proteins (experimental time ranging from 10 to 120 min per sample). The angle of the proton excitation pulse was set to 30°, and the recycling delay was optimized to 0.6 s to achieve the highest sensitivity.

The 3D HMQC-NOESY-HMQC experiment was recorded over 90 hours with a 75 μM (470 μM monomer) U-[^{2}H, ^{15}N], Met-[$^{13}CH_3$], Val-[$^{13}CH_3$]^{proS} sample of hsp60 with a nuclear Overhauser effect (NOE) mixing time of 600 ms (optimal NOE mixing time determined from the buildup of the cross-peak intensities in a series of short 2D NOESY spectra). NMR data were recorded on a Bruker Avance III HD spectrometer operating at a ^{1}H frequency of 950 MHz and equipped with a 5-mm cryogenically cooled pulsed-field gradient triple-resonance probes.

All the 2D (^{13}C,^{1}H)-DOSY NMR experiments were recorded on a Bruker Avance III HD spectrometer operating at a ^{1}H frequency of 700 MHz and equipped with a 5-mm cryogenically cooled pulsed-field gradient triple-resonance probes. A recycle delay of 1 s was used in all experiments. The diffusion time was set to 100 ms, gradient duration was 2 ms, and recovery delay was set to 0.2 ms, with a total acquisition time of 2 hours for each spectrum. The gradient strength varied from 5 to 42.5 G/cm.

^{13}C-edited 2D Exchange Spectroscopy (EXSY) experiments were acquired to characterize the exchange between folded and unfolded HEWL and to transfer assignment between the two forms. For this purpose, we have modified standard methyl-TROSY experiment (*17*) by adding a first 90° ^{1}H pulse just before proton acquisition to store magnetization along the *z* axis during the EXSY mixing delay. Then, the magnetization was flipped back in the transverse plane by the addition of a second 90° ^{1}H pulse for the detection of ^{1}H signal. All the 2D methyl-TROSY-EXSY experiments were acquired on a Bruker Avance III HD spectrometer operating at a ^{1}H frequency of 700 MHz equipped with a 5-mm cryogenically cooled pulsed-field gradient triple-resonance probe. A recycle delay of 1 s was used in all experiments. The EXSY mixing times were set to 1, 25, 50, 100, 200, 300, 500, 800, 1000, and 1300 ms, with an average acquisition time of 30 min for each spectrum.

Assignment of methyl group resonances

Assignment of HEWL Ile-δ_1, Val and Leu-proS methyl groups

Folded HEWL assignment was obtained from the published assignment (*36*). Unfolded HEWL assignment was transferred from the folded HEWL using a methyl-TROSY-EXSY experiment recorded at 65°C, where both unfolded and folded populations of HEWL can be observed (fig. S5D).

Assignment of hsp60 Met-ε and Val-γ2 methyl groups

Each mutant sample (40 μl) was loaded in a 1.7-mm tube, and the NMR experiments were recorded on a Bruker Avance III HD spectrometer operating at a ^{1}H frequency of 850 MHz and equipped with a 1.7-mm TCI MicroCryoProbe. The 2D SOFAST-methyl-TROSY NMR experiments (*18*) were recorded at 75°C with an adjusted duration depending on the final concentration of each mutant (experimental time ranging from 60 to 120 min per sample). For each mutant, spectra (fig. S1) were recorded for the apo state, App-NHp–bound state (1 mM), or ADP-bound state (1 mM). Analysis and comparison of the complete library of mutant spectra allowed the assignment of 33 valines (70%) and 15 methionines (100%). To obtain the missing assignment and confirm the assignment obtained by mutagenesis, a 3D HMQC-NOESY-HMQC experiment was recorded with a 47 μM (0.75 mM monomer) U-[^{2}H, ^{15}N], Met-[$^{13}CH_3$], Val-[$^{13}CH_3$]^{proS} sample of hsp60 (fig. S2). Comparison of the NOE cross peaks with the model of the structure of hsp60 allowed to confirm the mutagenesis assignment and to assign 43 valines (92%) and 15 methionines (100%).

Study of the interaction between client proteins and hsp60

Titration of the interaction between HEWL and hsp60

Spectra were recorded using a different sample for each titration point with a fixed concentration of 31 μM U-[^{2}H, ^{15}N], Val/Leu-[$^{13}CH_3$]^{proS}, Ile-[$^{13}CH_3$]$^{\delta1}$ HEWL and a variation of the concentration of U-[^{2}H, ^{15}N], Met-[$^{13}CH_3$] hsp60. Each sample (40 μl) was loaded in a 1.7-mm tube, and the NMR experiments were recorded on a Bruker Avance III HD spectrometer operating at a ^{1}H frequency of 850 MHz

and equipped with a 1.7-mm TCI MicroCryoProbe. The 2D SOFAST-methyl-TROSY NMR (*18*) experiments were recorded at 75°C.

Thermal unfolding of HEWL with and without hsp60

The reversible thermal (un)folding of HEWL (*37*) was probed using two samples. HEWL reference sample: 31 μM HEWL U-[^{2}H, ^{15}N], Val/Leu-[^{13}CH$_3$]^{proS}, Ile-[^{13}CH$_3$]$^{\delta1}$. HEWL with hsp60: 15 μM hsp60 (240 μM monomer concentration) U-[^{2}H, ^{15}N], Met-[^{13}CH$_3$] sample and 31 μM HEWL U-[^{2}H, ^{15}N], Val/Leu-[^{13}CH$_3$]^{proS}, Ile-[^{13}CH$_3$]$^{\delta1}$ sample (two equivalents of HEWL per hsp60 particle). Each sample (40 μl) was loaded in a 1.7-mm tube, and the NMR experiments were recorded on a Bruker Avance III HD spectrometer operating at a ^{1}H frequency of 850 MHz and equipped with a 1.7-mm TCI MicroCryoProbe. The 2D SOFAST-methyl-TROSY NMR experiments (*18*) were recorded from a temperature of 50° to 75°C with steps of 5°C between 50° and 60°C and steps of 2.5°C between 60° and 75°C. Percentage of folded state was extracted from the average ratio between the intensity of the signals in the folded and unfolded states for different residues.

Measurement of the translational diffusion coefficient of the free and hsp60-bound HEWL and MSG

For HEWL, three samples were used to acquire the 2D (^{13}C,^{1}H)-DOSY data sets (*40*) at a temperature of 65°C. Reference sample: 31 μM HEWL U-[^{2}H, ^{15}N], Val/Leu-[^{13}CH$_3$]^{proS}, Ile-[^{13}CH$_3$]$^{\delta1}$; hsp60 reference sample: 15.5 μM hsp60 (250 μM monomer concentration) U-[^{2}H, ^{15}N], Met-[^{13}CH$_3$]; and hsp60 with HEWL: 15,5 μM hsp60 (250 μM monomer concentration) U-[^{2}H, ^{15}N], Met-[^{13}CH$_3$] and 31 μM HEWL U-[^{2}H, ^{15}N], Val/Leu-[^{13}CH$_3$]^{proS}, Ile-[^{13}CH$_3$] $^{\delta1}$ sample (two equivalents of HEWL per hsp60 particle).

For MSG, three samples were used to acquire the 2D (^{13}C,^{1}H)-DOSY data sets. As thermally unfolded MSG is not soluble, the MSG reference spectrum was acquired at 50°C with 31 μM folded MSG U-[^{2}H, ^{15}N], Ile-[^{13}CH$_3$] $^{\delta1}$. For the sample containing unfolded MSG bound to hsp60, 15.5 μM hsp60 (250 μM monomer concentration) U-[^{2}H, ^{15}N], Met-[^{13}CH$_3$] was mixed to 31 μM MSG U-[^{2}H, ^{15}N], Ile-[^{13}CH$_3$] $^{\delta1}$. MSG was thermally unfolded at 60°C in the presence of hsp60 (two equivalents of MSG per hsp60 particle), and DOSY (Diffusion Ordered SpectroscopY) spectra were acquired at 60°C. The hsp60 reference sample spectrum was acquired at 60°C with a sample containing 15.5 μM hsp60 (250 μM monomer concentration) U-[^{2}H, ^{15}N], Met-[^{13}CH$_3$].

Paramagnetic labeling of HEWL and MSG for the detection of intermolecular paramagnetic relaxation enhancement (PRE) effects

Spin labeling of the ε-amino groups of the solvent accessible HEWL (Sigma-Aldrich) or MSG lysine residues with OXYL-1-NHS (1-oxyl-2,2,5,5-tetramethylpyrolline-3-carboxylate-*N*-hydroxysuccimide ester, Toronto Research Chemicals) was carried out following a published protocol (*41*). Protein was dissolved in the labeling buffer [10 mM Na_2CO_3 (pH 9.2)] at a concentration of 40 μM. A stock solution was prepared by dissolving 10 mg of OXYL-1-NHS in 100 μl of dimethyl sulfoxide. After addition of a sixfold molar excess of OXYL-1-NHS over lysine residues to the protein solution, the reaction mixture was incubated for 1 hour at room temperature, followed by 4 hours at 4°C. The excess of spin label was removed by washing the sample with approximately 20 volumes of NMR buffer using centrifugal filter devices (Vivaspin 15, 5000 MWCO, Vivascience). Homogeneity of the lysine labeling was checked by mass spectrometry.

We measured paramagnetic relaxation (PRE) enhancement values, to provide qualitative information on the interactions between HEWL or MSG and hsp60, by comparing peak intensities in 2D SOFAST-methyl-TROSY NMR experiments recorded at 75°C with a 16 μM hsp60 (256 μM monomer concentration) U-[^{2}H] Met-[^{13}CH$_3$], Val-[^{13}CH$_3$]^{proS} in interaction with either 32 μM OXYL-1-NHS–labeled ^{1}H HEWL (I_{ox})/MSG (I_{ox}) or reference diamagnetic HEWL (I_{red})/MSG (I_{red}). The reference sample was obtained by reducing the spin label of the OXYL-1-NHS–labeled sample by incubation with sodium ascorbate (2.2 mM) for 24 hours at 4°C. NMR data were recorded using a Bruker Avance III HD spectrometer operating at a ^{1}H frequency of 950 MHz and equipped with a 5-mm cryogenically cooled pulsed-field gradient triple-resonance probes.

NMR study of the hsp60 in action with/without HEWL

Sample conditions

Two samples were used to record the data. Hsp60 reference sample: 26 μM hsp60 (416 μM monomer concentration) U-[^{2}H, ^{15}N], Met-[^{13}CH$_3$]. Hsp60 with HEWL: 26 μM hsp60 (416 μM monomer concentration) U-[^{2}H, ^{15}N], Met-[^{13}CH$_3$] and 52 μM HEWL U-[^{2}H, ^{15}N], Val/Leu-[^{13}CH$_3$]^{proS}, Ile-[^{13}CH$_3$]$^{\delta1}$ (two equivalents of HEWL per hsp60 particle). All the samples were prepared in D_2O buffer containing 100 mM MES (pH 6.5 uncorrected), 100 mM NaCl, 150 mM KCl, and 25 mM $MgCl_2$.

Composition of the ATP regeneration system

ATP regeneration system was composed of 3 U of pyruvate kinase from *Bacillus stearothermophilus*, 0.1 mM ribulose-5-phosphate, and 220 mM PEP (Sigma-Aldrich).

Interleaved NMR experiments

The experiment was started by the addition of 10 mM ATP to the reaction mix, and the NMR tube was placed in the spectrometer at a temperature of 65°C. After an equilibration time of 5 min, 2D SOFAST-methyl-TROSY NMR spectra were recorded in interleaved mode with ^{1}H 1D spectra.

SUPPLEMENTARY MATERIALS

Supplementary material for this article is available at http://advances.sciencemag.org/cgi/content/full/4/9/eaau4196/DC1

Fig. S1. Examples of mutant spectra used to assign individual methionine and valine correlations.
Fig. S2. Cross-validation of the valine and methionine methyl group assignments.
Fig. S3. Interaction of hsp60 with different nucleotides.
Fig. S4. Conformational changes of hsp60 induced by a nonhydrolyzable ATP analog (App-NHp) investigated by EM and NMR.
Fig. S5. NMR characterization of the HEWL thermal unfolding without/with hsp60.
Fig. S6. Translational diffusion properties characterized by diffusion-ordered NMR spectroscopy.
Fig. S7. Determination of HEWL binding site on hsp60 using PRE experiments.
Fig. S8. Refolding of HEWL by ATP-powered chaperonin.
Fig. S9. Real-time NMR study of hsp60 functional cycle without client protein.
Fig. S10. Population of active hsp60 in ATP/ADP/apo state and closed/open state.
References (*42*–*45*)

REFERENCES AND NOTES

1. G. Kafri, A. Horovitz, Transient kinetic analysis of ATP-induced allosteric transitions in the eukaryotic chaperonin containing TCP-1. *J. Mol. Biol.* **326**, 981–987 (2003).
2. M. G. Bigotti, A. R. Clarke, Cooperativity in the thermosome. *J. Mol. Biol.* **348**, 13–26 (2005).
3. S. Reissmann, C. Parnot, C. R. Booth, W. Chiu, J. Frydman, Essential function of the built-in lid in the allosteric regulation of eukaryotic and archaeal chaperonins. *Nat. Struct. Mol. Biol.* **14**, 432–440 (2007).
4. A. Nakagawa, K. Moriya, M. Arita, Y. Yamamoto, K. Kitamura, N. Ishiguro, T. Kanzaki, T. Oka, K. Makabe, K. Kuwajima, M. Yohda, Dissection of the ATP-dependent conformational change cycle of a group II chaperonin. *J. Mol. Biol.* **426**, 447–459 (2014).

5. I. G. Muñoz, H. Yébenes, M. Zhou, P. Mesa, M. Serna, A. Y. Park, E. Bragado-Nilsson, A. Beloso, G. de Cárcer, M. Malumbres, C. V. Robinson, J. M. Valpuesta, G. Montoya, Crystal structure of the open conformation of the mammalian chaperonin CCT in complex with tubulin. *Nat. Struct. Mol. Biol.* **18**, 14–19 (2011).
6. J. H. Pereira, C. Y. Ralston, N. R. Douglas, D. Meyer, K. M. Knee, D. R. Goulet, J. A. King, J. Frydman, P. D. Adams, Crystal structures of a group II chaperonin reveal the open and closed states associated with the protein folding cycle. *J. Biol. Chem.* **285**, 27958–27966 (2010).
7. Y. Huo, Z. Hu, K. Zhang, L. Wang, Y. Zhai, Q. Zhou, G. Lander, J. Zhu, Y. He, X. Pang, W. Xu, M. Bartlam, Z. Dong, F. Sun, Crystal structure of group II chaperonin in the open state. *Structure* **18**, 1270–1279 (2010).
8. L. Ditzel, J. Löwe, D. Stock, K.-O. Stetter, H. Huber, R. Huber, S. Steinbacher, Crystal structure of the thermosome, the archaeal chaperonin and homolog of CCT. *Cell* **93**, 125–138 (1998).
9. Y. Zang, M. Jin, H. Wang, Z. Cui, L. Kong, C. Liu, Y. Cong, Staggered ATP binding mechanism of eukaryotic chaperonin TRiC (CCT) revealed through high-resolution cryo-EM. *Nat. Struct. Mol. Biol.* **23**, 1083–1091 (2016).
10. H. Yébenes, P. Mesa, I. G. Muñoz, G. Montoya, J. M. Valpuesta, Chaperonins: Two rings for folding. *Trends Biochem. Sci.* **36**, 424–432 (2011).
11. T. Lopez, K. Dalton, J. Frydman, The mechanism and function of group II chaperonins. *J. Mol. Biol.* **427**, 2919–2930 (2015).
12. M. Okochi, H. Matsuzaki, T. Nomura, N. Ishii, M. Yohda, Molecular characterization of the group II chaperonin from the hyperthermophilic archaeum *Pyrococcus horikoshii* OT_3. *Extremophiles* **9**, 127–134 (2005).
13. R. Sprangers, L. E. Kay, Quantitative dynamics and binding studies of the 20S proteasome by NMR. *Nature* **445**, 618–622 (2007).
14. J. Fiaux, E. B. Bertelsen, A. L. Horwich, K. Wüthrich, NMR analysis of a 900K GroEL–GroES complex. *Nature* **418**, 207–211 (2002).
15. R. Kerfah, M. J. Plevin, R. Sounier, P. Gans, J. Boisbouvier, Methyl-specific isotopic labeling: A molecular tool box for solution NMR studies of large proteins. *Curr. Opin. Struct. Biol.* **32**, 113–122 (2015).
16. A. M. Ruschak, L. E. Kay, Methyl groups as probes of supra-molecular structure, dynamics and function. *J. Biomol. NMR* **46**, 75–87 (2010).
17. V. Tugarinov, P. M. Hwang, J. E. Ollerenshaw, L. E. Kay, Cross-correlated relaxation enhanced $^{1}H–^{13}C$ NMR spectroscopy of methyl groups in very high molecular weight proteins and protein complexes. *J. Am. Chem. Soc.* **125**, 10420–10428 (2003).
18. C. Amero, P. Schanda, M. Asunción Durá, I. Ayala, D. Marion, B. Franzetti, B. Brutscher, J. Boisbouvier, Fast two-dimensional NMR spectroscopy of high molecular weight protein assemblies. *J. Am. Chem. Soc.* **131**, 3448–3449 (2009).
19. R. Iizuka, T. Yoshida, Y. Shomura, K. Miki, T. Maruyama, M. Odaka, M. Yohda, ATP binding is critical for the conformational change from an open to closed state in archaeal group II chaperonin. *J. Biol. Chem.* **278**, 44959–44965 (2003).
20. J. Zhang, M. L. Baker, G. F. Schröder, N. R. Douglas, S. Reissmann, J. Jakana, M. Dougherty, C. J. Fu, M. Levitt, S. J. Ludtke, J. Frydman, W. Chiu, Mechanism of folding chamber closure in a group II chaperonin. *Nature* **463**, 379–383 (2010).
21. J. Zhang, B. Ma, F. DiMaio, N. R. Douglas, L. A. Joachimiak, D. Baker, J. Frydman, M. Levitt, W. Chiu, Cryo-EM structure of a group II chaperonin in the prehydrolysis ATP-bound state leading to lid closure. *Structure* **19**, 633–639 (2011).
22. C. R. Booth, A. S. Meyer, Y. Cong, M. Topf, A. Sali, S. J. Ludtke, W. Chiu, J. Frydman, Mechanism of lid closure in the eukaryotic chaperonin TRiC/CCT. *Nat. Struct. Mol. Biol.* **15**, 746–753 (2008).
23. O. Llorca, J. Martín-Benito, J. Grantham, M. Ritco-Vonsovici, K. R. Willison, J. L. Carrascosa, J. M. Valpuesta, The "sequential allosteric ring" mechanism in the eukaryotic chaperonin-assisted folding of actin and tubulin. *EMBO J.* **20**, 4065–4075 (2001).
24. I. Gutsche, J. Holzinger, N. Rauh, W. Baumeister, R. P. May, ATP-induced structural change of the thermosome is temperature-dependent. *J. Struct. Biol.* **135**, 139–146 (2001).
25. A. S. Meyer, J. R. Gillespie, D. Walther, I. S. Millet, S. Doniach, Closing the folding chamber of the eukaryotic chaperonin requires the transition state of ATP hydrolysis. *Cell* **113**, 369–381 (2003).
26. N. R. Douglas, S. Reissmann, J. Zhang, B. Chen, J. Jakana, R. Kumar, W. Chiu, J. Frydman, Dual action of ATP hydrolysis couples lid closure to substrate release into the group II chaperonin chamber. *Cell* **144**, 240–252 (2011).
27. H.-y. Chen, X.-l. Tan, J. Lu, C.-x. Zhang, Y. Zhang, S.-l. Yang, Characterization of ATPase activity of class II chaperonin from the hyperthermophilic archaeon *Pyrococcus furiosus*. *Biotechnol. Lett.* **31**, 1753–1758 (2009).
28. A. R. Kusmierczyk, J. Martin, Nested cooperativity and salt dependence of the ATPase activity of the archaeal chaperonin Mm-cpn. *FEBS Lett.* **547**, 201–204 (2003).
29. G. Kafri, K. Y. Willison, A. Horovitz, Nested allosteric interactions in the cytoplasmic chaperonin containing TCP-1. *Protein Sci.* **10**, 445–449 (2001).
30. A. Horovitz, Y. Fridmann, G. Kafri, O. Yifrach, Review: Allostery in chaperonins. *J. Struct. Biol.* **135**, 104–114 (2001).
31. M. G. Bigotti, S. R. W. Bellamy, A. R. Clarke, The asymmetric ATPase cycle of the thermosome: Elucidation of the binding, hydrolysis and product-release steps. *J. Mol. Biol.* **362**, 835–843 (2006).
32. P. Lin, F. Sherman, The unique hetero-oligomeric nature of the subunits in the catalytic cooperativity of the yeast Cct chaperonin complex. *Proc. Natl. Acad. Sci. U.S.A.* **94**, 10780–10785 (1997).
33. D. Rivenzon-Segal, S. G. Wolf, L. Shimon, K. R. Willison, A. Horovitz, Sequential ATP-induced allosteric transitions of the cytoplasmic chaperonin containing TCP-1 revealed by EM analysis. *Nat. Struct. Mol. Biol.* **12**, 233–237 (2005).
34. A. Horovitz, K. R. Willison, Allosteric regulation of chaperonins. *Curr. Opin. Struct. Biol.* **15**, 646–651 (2005).
35. J. Wu, T. Liu, Z. Rios, Q. Mei, X. Lin, S. Cao, Heat shock proteins and cancer. *Trends Pharmacol. Sci.* **38**, 226–256 (2017).
36. Z. Gu, Z. Su, J.-C. Janson, Urea gradient size-exclusion chromatography enhanced the yield of lysozyme refolding. *J. Chromatogr. A* **918**, 311–318 (2001).
37. H. Schwalbe, S. B. Grimshaw, A. Spencer, M. Buck, J. Boyd, C. M. Dobson, C. Redfield, L. J. Smith, A refined solution structure of hen lysozyme determined using residual dipolar coupling data. *Protein Sci.* **10**, 677–688 (2001).
38. B. Ojha, N. Fukui, K. Hongo, T. Mizobata, Y. Kawata, Suppression of amyloid fibrils using the GroEL apical domain. *Sci. Rep.* **6**, 31041 (2016).
39. C. Schlörb, K. Ackermann, C. Richter, J. Wirmer, H. Schwalbe, Heterologous expression of hen egg white lysozyme and resonance assignment of tryptophan side chains in its non-native states. *J. Biomol. NMR* **33**, 95–104 (2005).
40. T. Didenko, R. Boelens, S. G. D. Rüdiger, 3D DOSY-TROSY to determine the translational diffusion coefficient of large protein complexes. *Protein Eng. Des. Sel.* **25**, 319 (2012).
41. F. Meersman, C. Atilgan, A. J. Miles, R. Bader, W. Shang, A. Matagne, B. A. Wallace, M. H. J. Koch, Consistent picture of the reversible thermal unfolding of hen egg-white lysozyme from experiment and molecular dynamics. *Biophys. J.* **99**, 2255–2263 (2010).
42. J.-J. Lawrence, L. Berne, J. L. Ouvrier-Buffet, L. H. Piette, Spin-label study of histone H1–DNA interaction. *Eur. J. Biochem.* **107**, 263–269 (1980).
43. C. D. Amero, M. A. Durá, M. Noirclerc-Savoye, A. Perollier, B. Gallet, M. J. Plevin, T. Vernet, B. Franzetti, J. Boisbouvier, A systematic mutagenesis-driven strategy for site-resolved NMR studies of supramolecular assemblies. *J. Biomol. NMR* **50**, 229–236 (2011).
44. E. Crublet, R. Kerfah, G. Mas, M. Noirclerc-Savoye, V. Lantez, T. Vernet, J. Boisbouvier, A cost-effective protocol for the parallel production of libraries of $^{13}CH_3$-specifically labeled mutants for NMR studies of high molecular weight proteins. *Methods Mol. Biol.* **1091**, 229–244 (2014).
45. G. Mas, E. Crublet, O. Hamelin, P. Gans, J. Boisbouvier, Specific labeling and assignment strategies of valine methyl groups for NMR studies of high molecular weight proteins. *J. Biomol. NMR* **57**, 251–262 (2013).

Acknowledgments: The authors thank B. Brutscher, I. Gutsche, and S. Hiller for the stimulating discussions and comments on the manuscript. **Funding:** This work used the high-field NMR and EM facilities at the Grenoble Instruct-ERIC Center (ISBG; UMS 3518 CNRS CEA-UJF-EMBL) with support from the French Infrastructure for Integrated Structural Biology (FRISBI; ANR-10-INSB-05-02) and the Grenoble Alliance for Integrated Structural Cell Biology (GRAL; ANR-10-LABX-49-01) within the Grenoble Partnership for Structural Biology. The electron microscope facility is supported by the Rhône-Alpes Region, the Fondation Recherche Medicale (FRM), the Fonds Européen de Développement Régional, and the GIS–Infrastrutures en Biologie Santé et Agronomie (IBISA). This work was supported by the European Research Council (ERC-StG-2012-311318 and ERC-CoG-2010-260887). **Author contributions:** J.B., G.M., P.M., and P.S. designed the experiments, analyzed the results, and wrote the manuscript. G.M., J.-Y.G., E.C., and E.C.D. prepared the samples. C.M. and G.S. performed the EM experiments. G.M., J.-Y.G., E.C., E.C.D., J.B., P.G., P.M., and P.S. performed the NMR experiments. **Competing interests:** The authors declare that they have no competing interests. **Data and materials availability:** All data needed to evaluate the conclusions in the paper are present in the paper and/or the Supplementary Materials. Additional data related to this paper may be requested from the authors.

Submitted 8 June 2018
Accepted 1 August 2018
Published 19 September 2018
10.1126/sciadv.aau4196

Citation: G. Mas, J.-Y. Guan, E. Crublet, E. C. Debled, C. Moriscot, P. Gans, G. Schoehn, P. Macek, P. Schanda, J. Boisbouvier, Structural investigation of a chaperonin in action reveals how nucleotide binding regulates the functional cycle. *Sci. Adv.* **4**, eaau4196 (2018).